12th International Symposium on Turbulence and Shear Flow Phenomena (TSFP12)
Osaka, Japan (Online), July 19-22, 2022

ON THE SPECTRAL DECOMPOSITION OF SKEWNESS IN CANONCIAL AND ACTUATED TURBULENT BOUNDARY LAYERS

S. Midya,
Institute for Flow Physics and Control
University of Notre Dame
Notre Dame, IN
Samaresh.Midya.1@nd.edu

F. O. Thomas
Institute for Flow Physics and Control
University of Notre Dame
Notre Dame, IN
fthomas@nd.edu

S. V. Gordeyev
Institute for Flow Physics and Control
University of Notre Dame
Notre Dame, IN
sgordeye@nd.edu

ABSTRACT

The skewness of the streamwise velocity is an important parameter in turbulent boundary layer flows. It is intrinsically related to the mechanism of quadratic energy transfer between different scales of motion and has also been shown to be related to the modulation of near-wall turbulence by large scales. In this paper, the skewness in both a canonical and actuated zero pressure gradient turbulent boundary layer is spectrally decomposed via the real part of the bispectrum. It is shown that the real part of the bispectrum allows the individual triad interactions contributing to the skewness to be analyzed. These measurements are presented for a range of wall-normal locations associated with positive, zero and negative skewness. The individual contributions are also summed to obtain partial and cumulative sums of the skewness as a function of frequency. Complementary conditional sampling measurements demonstrate that the main contribution to boundary layer skewness is intimately associated with ejection-sweep events and the degree of asymmetry of their characteristic velocity signatures. Actuation is used to document the influence of outer layer large-scale structures on the spectral content of skewness.

INTRODUCTION

It is clear that the skewness of the streamwise velocity fluctuation is an important parameter in turbulent boundary layers (TBL). It is intrinsically related to the quadratic energy transfer mechanism since only triadically coupled modes make non-zero contributions to the skewness (Duvvuri & Mckeon, 2015). Skewness is also intimately related to the interactions between different spatial scales present in the turbulent flow. Hutchins and Marusic (2007a,b) demonstrated that near wall turbulence is modulated by the outer large-scale motions. This amplitude modulation of near wall turbulence was characterized by Mathis et al (2009, 2011). Their study correlated a low-pass filtered outer region signal with the envelope function of the near-wall, small-scale velocity fluctuations obtained via a Hilbert transform. The resulting profile of the normalized amplitude modulation correlation coefficient was found to bear a very strong resemblance to the corresponding velocity skewness profile. Using a scale decomposed signal given by $u+ = u_L^+ + u_S^+$ where subscripts L and S denote large- and small-scale contributions, respectively, they showed that a significant contribution to the skewness is the cross term $3\overline{u_L^+ u_S^+}$ where an overbar indicates a time-mean quantity. Given this importance, this paper examines the spectral decomposition of the skewness in a zero-pressure gradient turbulent boundary layer. This decomposition is achieved via the real part of the bispectrum and provides a measure of the modal contribution to the skewness at different representative wall-normal locations. The relation between the skewness and the bispectrum is described in the following section.

THE SPECTRAL DECOMPOSITION OF SKEWNESS

Like the spectral decomposition of the second moment via the autospectral density, one can decompose the skewness in frequency domain using the third-order spectral estimate known as the bispectrum. The bispectrum captures the triadic interactions between the frequencies present in the flow. The bispectrum is defined as,

$$B_{xxx}\left(f_1^*, f_2^*\right) = E\left[\hat{X}^C_{f^*} \hat{X}_{f_1^*} \hat{X}_{f_2^*}\right]$$

where

$$f^* = f_1^* + f_2^*$$

Here, $E[\ ]$ denotes an expected value, $\hat{x}_{f_1^*}$ a temporal Fourier transform of a time series $x(t)$ and the superscript C denotes a complex conjugate. In the application of the bispectrum to be used in the boundary layer here, the frequencies have been normalized by the large eddy frequency ($f_i^* \equiv f_i\, \delta / U_\infty$). Owing to its symmetry properties (e.g Rosenblatt and Ness (1965), Kim and Powers 1979, Elgar (1987)) it is sufficient to compute the bispectrum for the triangular frequency domain shown in Figure 1. This triangular region is associated with triad sum interactions. The correspodning two difference interactions involving the same wave triad would also map to the same point in this domain. For the triangular region shown in Figure 1, the third moment is related to the real part of the bispectrum by the relation (Rosenblatt and Ness (1965), Elgar and Guza (1985)),

$$E\left(u^3(t)\right) = 12\sum_{f_1^*} \sum_{f_2^* < f_1^*} \mathrm{Re}\left(B_{xxx}\left(f_1^*, f_2^*\right)\right) + 6\sum_{f_1^*} \mathrm{Re}\left(B_{xxx}\left(f_1^*, f_2^*\right)\right)$$

This equation can be normalized by u_{rms}^3 in order to directly relate the real part of the bispectrum to skewness. The real part of the bispectra to be presented were computed form signals normalized by u_{rms}^3.

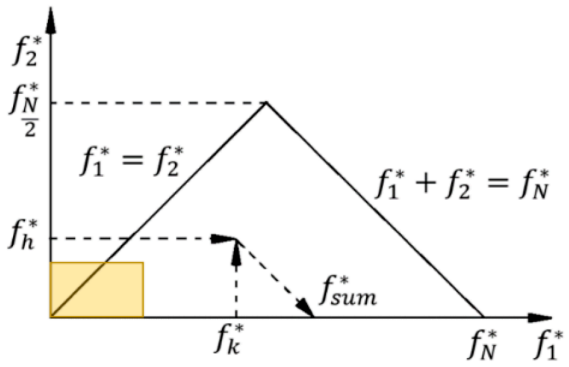

Figure 1. Region of computation of the auto-bispectrum. Only the sum interaction region is shown.

EXPERIMENTAL FACILITY

The experiments were conducted in a subsonic, open-return wind tunnel in the Hessert Laboratory at the University of Notre Dame. The wind tunnel has an inlet with a contraction ratio of 20:1. The inlet has a series of 12 turbulence management screens to condition the flow resulting in freestream turbulence levels of less than 0.1% for frequencies greater than 10 Hz. The test section is 0.61 m by 0.61 m in cross section and 1.83 m in length. A flat boundary layer development plate 2 meters in length with an elliptic leading edge covered with distributed sandgrain roughness was installed in the tunnel. The plate spanned the full width of the test section. Hot-wire traverses confirmed canonical zero pressure gradient TBL development on the plate. Table 1 summarizes the boundary layer parameters measured 1.42 m downstream of the plate leading edge.

Table 1. Turbulent Boundary Layer Parameters

δ	U_∞	u_τ	C_f	H	Re_θ	Re_τ
35 mm	7.0 m/s	0.298 m/s	0.0037	1.3	1,770	690

In order to introduce *organized* large-scale spanwise vorticity into the boundary layer, a plasma-based Active Large-Scale Structure Actuator (ALSSA) was developed and used (see Lozier et al, 2020, 2022). The ALSSA uses AC-DBD plasma to introduce organized large-scale coherent structures into the TBL. Figure 2 shows a schematic of the setup. The actuator consists of thin plate of streamwise length δ (the boundary layer thickness), spanwise length 8δ and maximum thickness of 0.05δ, with its trailing 0.3δ linearly tapered. The contoured elliptic leading edge of the plate was located at a streamwise distance of x =140 cm from the boundary layer development plate leading edge. The plate was placed at a wall normal location of h = 0.3δ (h^+ = 200). The spanwise length chosen ensured spanwise homogeneity. The plate was made of Ultem (dielectric material) to facilitate the plasma generation. The DBD plasma was operated with a 4kV carrier frequency with 32kV peak-to-peak voltage and was modulated with a square wave at a frequency of 80Hz (f^* = 0.4) with 50% duty cycle. This introduced a series of spanwise vortices at passage frequency f^* = 0.4 into the TBL at y^+ = 200. The resulting modal velocity is shown in Figure 10 of Lozier et al (2020, 2022).

For the canonical turbulent boundary layer at $Re_\theta = 1770$, the Reynolds number was sufficiently low that the pre-multiplied 1-D wavenumber spectra showed no dominant outer peak. In this manner, the ALSSA could be used to introduce periodic coherent structures into the outer region as described in Lozier et al (2021, 2022). This allowed examination of their influence on the nature and spectral decomposition of skewness.

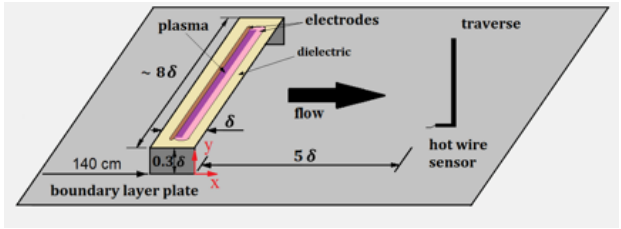

Figure 2. Schematic of the ALSSA actuator mounted on the boundary layer development plate.

Figure 3 compares skewness profiles for the canonical and plasma-actuated turbulent boundary layer cases. This figure shows similar skewness profile shapes for both cases. However, somewhat higher positive skewness occurs near the wall for the plasma actuated case. Both profiles reach near zero skewness at y^+ = 15 with the plasma actuated case showing greater negarive skewness in the lower logarithmic region.

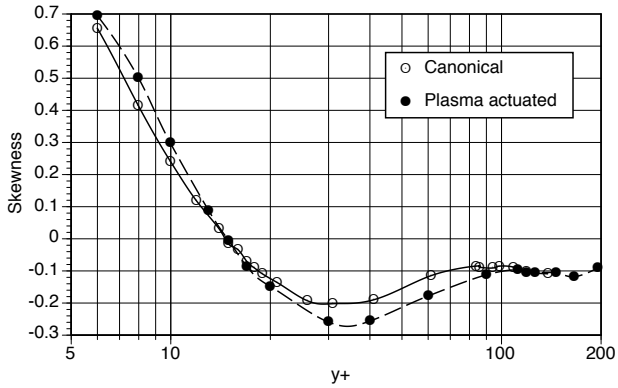

Figure 3. Skewness profiles for the canonical and plasma-actuated turbulent boundary layers.

SPECTRAL DECOMPOSITION OF SKEWNESS IN THE TURBULENT BOUNDARY LAYER

The location y^+ = 8 is taken as representative of the positive skewness that is observed in the near-wall region of turbulent boundary layers over a wide range of Reynolds numbers and the spectral decomposition for the canonical boundary layer case is shown in Figure 4a. The real part of the bispectrum is presented in an f_1^*, f_2^*, sub-domain (highlighted by the colored rectangular region in Figure 1) that is a smaller subset of the full domain in order to highlight the region of significant modal content. For all bispectral computations, a sampling frequency of 30 kHz ($f_{sample}^* = 150$), an FFT blocksize of 8192 and total 1300 blocks were used for the calculations. A series of convergence tests were performed in order to verify that all bispectra were fully converged.

The variable-interval-time-averaging (VITA) conditional sampling technique of Blackewelder and Kaplan (1976) was also applied but a distinction was made in the conditional sampling algorithm between ejection-sweep (ES) events

leading to positive versus negative skewness. The ES signatures that gives rise to negative skewness are denoted by -Ve and those giving rise to positive skewness are denoted +Ve. For comparative purposed Figure 4b presents the probability density functions (PDF) at $y^+ = 8$ for VITA ES event frequency, f^*, that result in either positive or negative skewness. The PDF for positive skewness events is indicated in red while that associated with negative skewness is indicated in green and overlays the +Ve with sufficient transparency so that its PDF can still be discerned. It is quite clear that at $y^+=8$ positive skewness ES events are much more frequent which is fully consistent with the positive skewness shown in Figure 3 for the $y^+=8$ location.

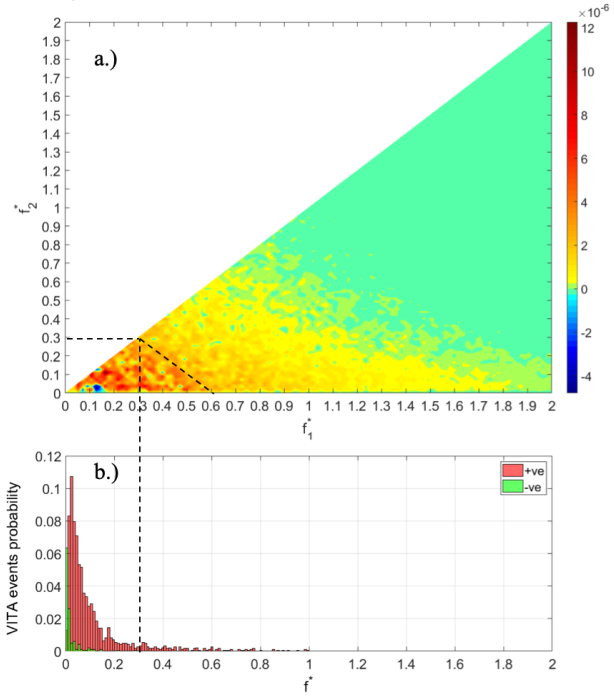

Figure 4. a) Spectral decomposition of skewness at $y^+=8$ for the canonical TBL. b) PDF of the frequency of positive (+Ve) and negative (-Ve) skewness producing E-S events.

Figure 4a shows that the most significant triad interactions contributing to positive near-wall skewness at $y^+ = 8$ involve f_1^* and $f_2^* < 0.3$. That is, the region of most significant triad interactions is bounded by $f_1^* + f_2^* = 0.6$ as indicated by the triangular region delineated by the dashed lines. Figure 4b shows this to correspond to the frequency range contributing most to the probability density function for the frequency of +Ve burst events. Based on the VITA conditional sampling, the mean positive skewness event frequency at $y^+ = 8$ is approximately $f_{+ve}^* = 0.05$. It may be noted from Figure 4a that the highest peaks of the real portion of the bispectrum lie inside the dashed region with triad interactions that involve multiples of this frequency: $(i/2)\, f_{+ve,1}^* + (j/2)\, f_{+ve,2}^*$, $i = 2,3,4,5$ $j = 2,3,4,5$. Figure 4a also shows that weaker triad interactions involving $f_1^* = f_2^* < 0.7$, which conicides with the upper limit of frequency content of the PDF for VITA ES event frequency, also contribute to the positive skewness.

Figure 5a presents the spectal decomposition of skewness at $y^+ = 8$ for the ALLSA actuated TBL. Figure 5b presents the corresponmding PDFs at $y^+ = 8$ for VITA ES event frequency, that result in either positive or negative skewness. With actuation, the most probable frequency for positive and negative producing ES events is $f_{+ve}^* = 0.04$ and $f_{-ve}^* \approx 0.003$, respectively. As in the canonical TBL, the dominant triad interactions involve involve f_1^* and $f_2^* < 0.3$ as indicated by the dashed triangular region in Figure 5a. The peak triad interactions in this region are associated with integer multiples of f_{+ve}^*. A main difference of the spectral decomposition for the actuated TBL are the indicated triad interactions associated with actuation frequency $f^* = 0.4$ and a range of frequencies extending to $f^* = 1.5$ as indicated by the arrows in Figure 5a. These triad interactions are associated with the production of positive skewness.

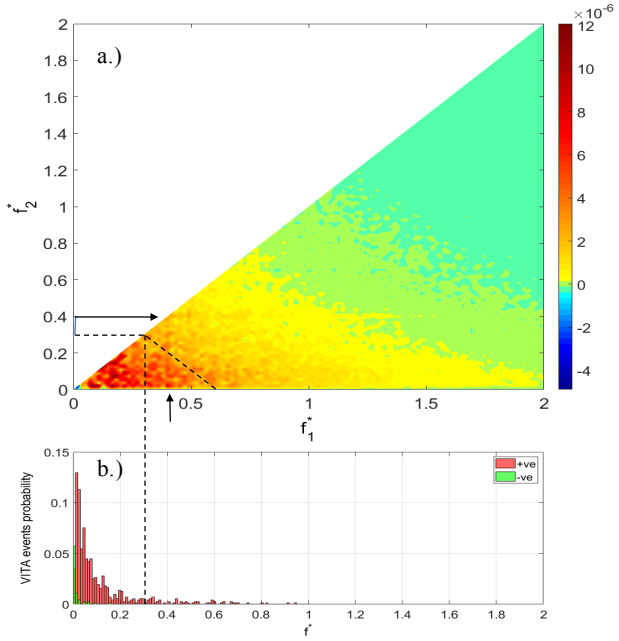

Figure 5. a) Spectral decomposition of skewness at $y^+=8$ for the actuated TBL. b) PDF of the frequency of positive (+Ve) and negative (-Ve) skewness producing E-S events.

A summation over the real part of the bispectrum recovers the skewness. Figure 6 shows the method of summation over the real part of the bispectrum. The frequency resolution, Δf_1^* and Δf_2^* of the bispectral plot are set equal. As shown in Figure 6a the area is divided using lines connecting $(i\,\Delta f_1^*, 0)$ and $(0, i\Delta f_2^*)$ (where $i = 1,2,..,N$). The sum is taken over the

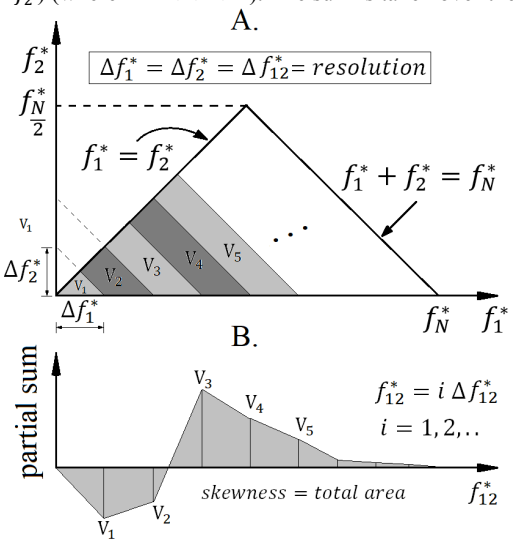

Figure 6. Summation over the real part of the bispectrum to recover skewness.

region between a pair of consecutive lines and is denoted by V_i (where $i = 1,2,..,N$). These values can then be plotted as a partial sum as shown in Figure 6b. The abscissa is denoted f_{12}^* and its resolution Δf_{12}^* equals Δf_1^*. Thus, the area under the curve of V_is recovers the skewness.

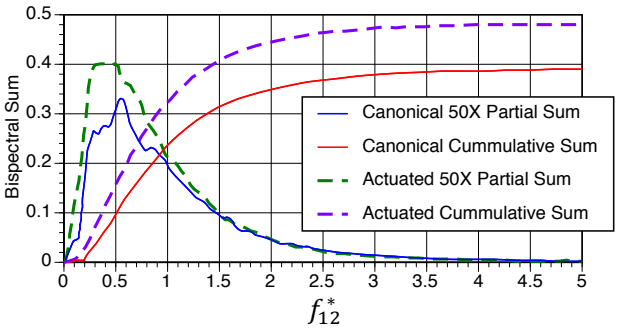

Figure 7. Partial and cumulative bispectral sums for the canonical and actuated TBL at y^+ =8.

Figure 7 compares the partial and cumulative bispectral sums for the canonical and actuated TBLs at y^+=8. Both exhibit similar partial bispectral sum variations with f_{12}^*. The dominance of triad interactions producing positive skewness is readily apparent. The canonical case peaks near f_{12}^*= 0.6 and the actuated case near f_{12}^*=0.5. In both cases this is associated with the dominant triad interactions within the dashed regions shown in Figures 4a and 5a.

Figure 8a presents the spectral decomposition of skewness at y^+ = 15 for the canonical TBL. The corresponding PDFs for the frequency of positive (+Ve) and negative (-Ve) skewness producing ES events is shown in Figure 8b. It is clear from this figure that at this wall normal location the relative frequency of both type of events is now comparable. More specifically,

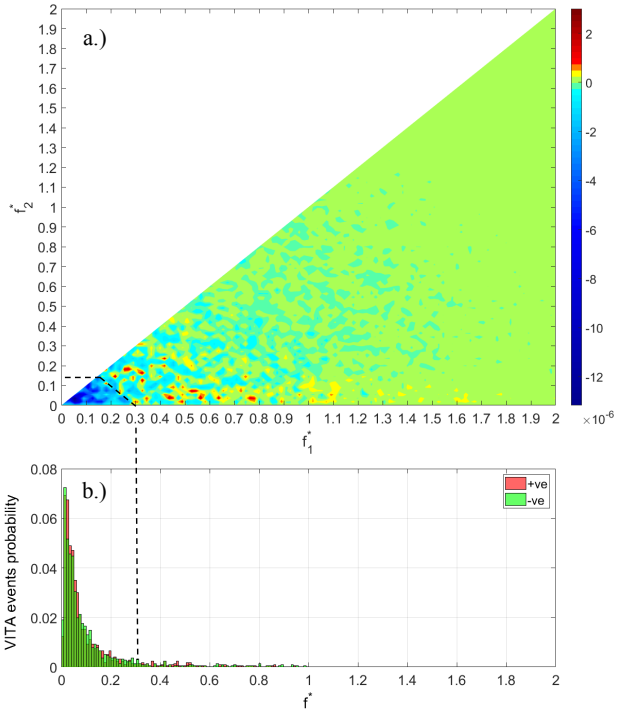

Figure 8. a) Spectral decomposition of skewness at y^+=15 for the canonical TBL. b) PDF of the frequency of positive (+Ve) and negative (-Ve) skewness producing E-S events.

$f_{+ve}^* = 0.031$ and $f_{-ve}^* = 0.029$. This is consistent with the observation from Figure 3 that the skewness is nearly zero at this wall-normal location. Figure 8a shows that as before, the dominant interactions are clearly associated with the frequency range shown in the PDFs for +Ve and -Ve events ($f_1^*, f_2^* < 0.3$). Negative peaks are now present in this region for $f_1^* < 0.3$ and $f_2^* < 0.15$. Examination of the ordinate scale shows that the negative peaks clearly dominate the positive peaks in this region.

Figure 9a presents the spectral decomposition of skewness at y^+ =15 for the actuated TBL. The corresponding PDFs for the positive and negative skewness producing ES events are shown in Figure 9b. As in the canonical flow the most probable frequencies for positive and negative skewness producing events are comparable: $f_{+ve}^* = 0.034$ and $f_{-ve}^* = 0.038$. As was the case for the canonical TBL, negative peaks dominate the bispectrum for $f_1^* < 0.3$ and $f_2^* < 0.15$. The influence of the ALLSA-imposed outer large-scale structures is manifest in multipe triad interactions between $f^* = 0.4$ and a range of frequencies extending to $f^* = 1.7$ although the strongest occur for $f^* < 0.6$.

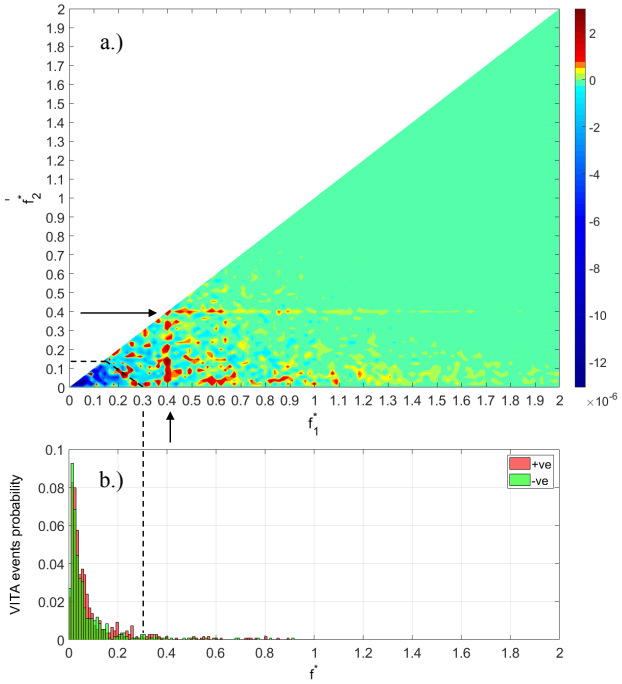

Figure 9. a) Spectral decomposition of skewness at y^+=15 for the actuated TBL. b) PDF of the frequency of positive (+Ve) and negative (-Ve) skewness producing E-S events.

Figure 10 compares the partial and cumulative bispectral sums for the canonical and actuated TBLs at y^+=15. The dominance of the negative skewness producing triad interactions shown in the dashed triangular regions in Figures 8a and 9a is apparent and both the actuated and canonical partial sums show negative peak values centered near f_{12}^*=0.2. The primary difference between the two cases is associated with multiple triad interactions between $f^* = 0.4$ and a range of frequencies extending to $f^* = 1.7$ for the actuated case. This gives rise to positive peaks in the actuated case partial sum leading to nearly zero skewness. In contrat, the canonical case cummulative sum remains negative.

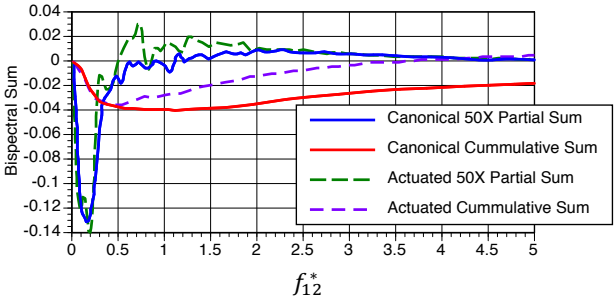

Figure 10. Partial and cumulative bispectral sums for the canonical and actuated TBL at y^+ =15.

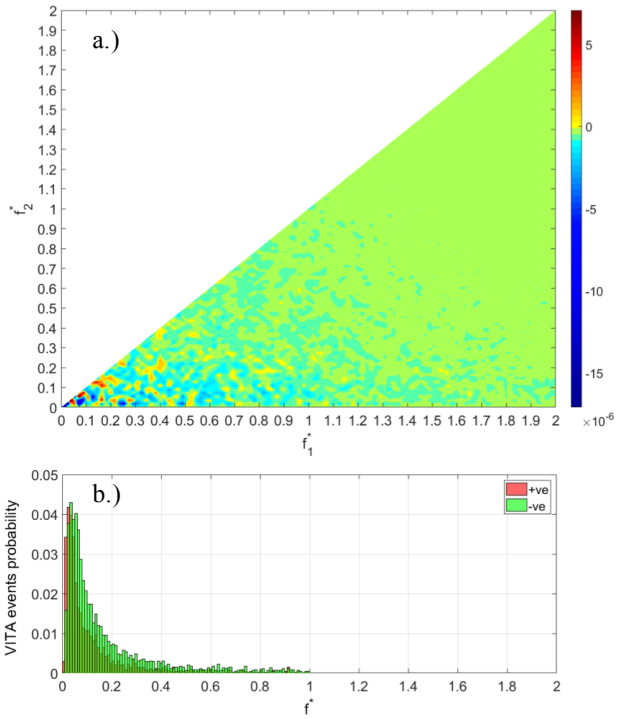

Figure 11. a) Spectral decomposition of skewness at y^+=60 for the canonical TBL. b) PDF of the frequency of positive (+Ve) and negative (-Ve) skewness producing E-S events.

The spectral decomposition of skewness for the canonical TBL at y^+ = 60 is shown in Figure 11a and demonstrates a clear dominance of triad interactions producing negative skewness. The corresponding PDFs obtained at y^+ = 60 for the frequency of both +Ve, positive and -Ve, negative skewness producing ES events are presented in Figure 11b. This figure shows the significantly increased frequency of negative skewness producing events relative to those producing positive skewness. The mean frequency for +Ve events is f_{+ve}^* = 0.049 and for -Ve events, f_{-ve}^* = 0.076 at this location. The dominant interactions shown in the spectral decomposition involve multiples of the mean frequencies for both +Ve and -Ve events with interactions producing negative skewness dominating.

Figure 12a presents the spectral decomposition of skewness for the actuated TBL at y^+ = 60. The corresponding PDFs for the frequency of ES events producing positive and negative skewness are shown in Figure 12b. As was the cse in the canonical flow, the mean frequency of negative skewness events (f_{-ve}^* = 0.085) exceeds that for positive skewness producing evetns (f_{-ve}^* = 0.053). Consistent with this, triad interactions associated with negative skewness dominate the spectral decomosition over the frequency band associated with the PDFs of ES events. The effect of the actuated large-scale structures imposed by ALLSA is also now readlily apparent and gives rise to triad interactions producing positive skewness for f_2^* < 0.4 and f_1^* > 0.2.

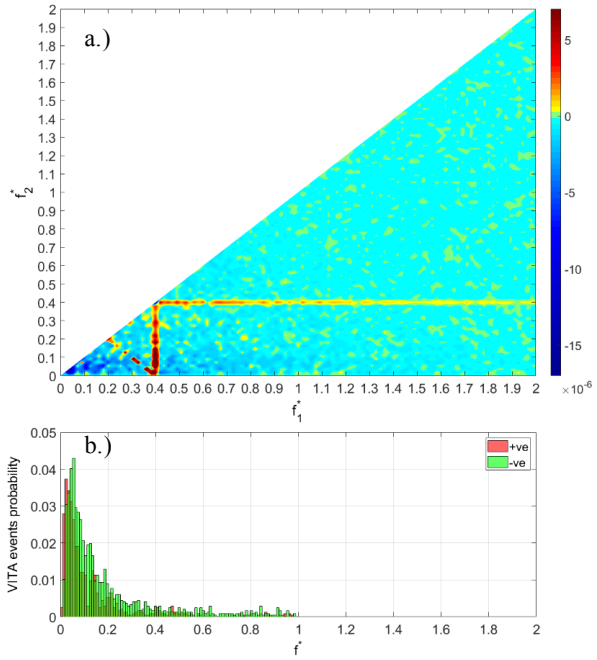

Figure 12. a) Spectral decomposition of skewness at y^+=60 for the actuated TBL. b) PDF of the frequency of positive (+Ve) and negative (-Ve) skewness producing E-S events.

Figure 13 compares the partial and cumulative bispectral sums for the canonical and actuated TBLs at y^+=60. This location is within the lower logarithmic region of the mean velocity profile (the center of the logarithmic region is given by $y^+ = \sqrt{15\,Re_\tau} = 102$). In this case the influence of the introduced large-scale structures is quite significant. The canonical case is dominated by triad interactions producing negative skewness over a wide range in frequency. In contrast, the influence of the imposed large-scale structures gives rise to a series of triad interactions (Figure 12a) that produces a positive peak in the partial skewness summation at $f_{12}^* = 0.4$. It is also apparent that the imposed structures exacerbate the negative triad interactions such that the cumulative sum for the actuated case is more negative than in the canonical flow.

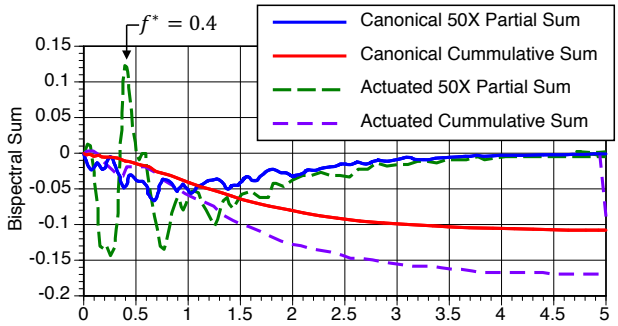

Figure 13. Partial and cumulative bispectral sums for the canonical and actuated TBL at y^+=60.

Figure 14 presents the phase-averaged skewness (mean removed) in the actuated boundary layer. Here $\tilde{u}$ denotes the periodic modal component due to the imposed periodic actuation and u the residual turbulence. This figure clearly shows that the artifically introduced outer large-scale structures at y^+ =200 modulate the skewness. Although this effect extends to near the wall, it is much more pronounced in the logarithmic region. Hence, as shown in the spectral decomposition measurements, even in the actuated boundary layer the skewness is largely dominated by discrete ES events associated with buffer layer streamwise vorticity.

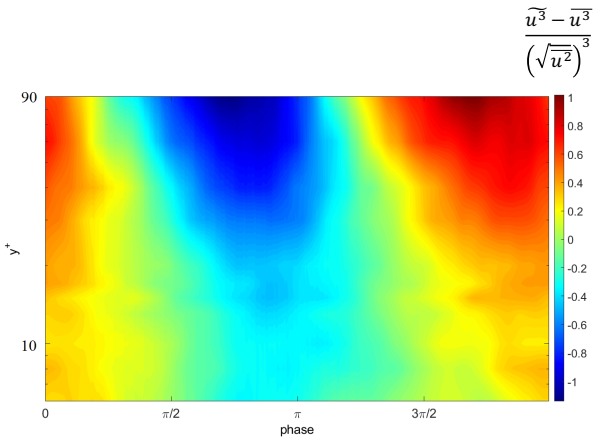

Figure 14. Phase-averaged skewness (mean removed) in the actuated turbulent boundary layer.

CONCLUSION

The real part of the bispectrum is used to spectrally decompose the skewness of streamwise fluctuating velocity in both a canonical zero pressure gradient TBL and for the case in which the ALLSA actuator (Lozier et al, 2020, 2022) introduces organized vortical motions into the TBL at y^+ =200. In both cases Re_θ = 1,770. The Reynolds number is sufficiently low that a naturally occurring dominant outer turbulence intensity peak does not exist in the 1D pre-multiplied streamwise wavenumber spectrum (Midya, 2021). Comparison of the spectral decomposition for the natural and actuated turbulent boundary layer is performed at three wall-normal locations: y^+ = 8, which represents a region of positive skewness in the near-wall region; y^+ = 15 which corresponds to the wall normal location of peak turbulence intensity and for which the skewness is near zero; y^+ = 60 which represents the lower logarithmic region. Supporting conditional measurements show that the triad interactions responsible for near-wall skewness are intimately tied to the frequencies associated with positive and negative skewness producing ejection-sweep events. This suggests the important role played by buffer layer streamwise vorticity in near-wall TBL skewness. Furthermore, the imposition of large-scale vortical structures into the logarithmic region via ALLSA has little effect on the spectral distribution of skewness at y^+ = 8 and only a modest effect at y^+ = 15 with the observed triad interactions remaining dominated by those associated with positive or negative skewness producing ejection-sweep events. In contrast, the effect of the actuation becomes quite significant at y+ = 60 where triad interactions associated with the presence of coherent structures with passage frequency f^* = 0.4 become readily apparent and significantly effect the skewness.

These results suggest a near-wall autonomous mechanism associated with the production of buffer layer vorticity whose role in near-wall skewness dominates. Along with this is the combined effect of modulation by outer large-scale structures whose effect on skewness grows with distance from the wall. The increased effect of large-scale modulation with distance from the wall is apparent in the phase averaged skewness shown in Figure 14.

REFERENCES

Blackwelder, R.F., Kaplan, R.E. On the wall structure of the turbulent boundary layer, 1976, J. Fluid Mech., Vol. 76, pp. 89-112.

Duvvuri, S., and McKeon, B., “Phase relations in a forced turbulent boundary layer: implications for modelling of high Reynolds number wall turbulence”. Philos Trans A Math Phys Eng Sci., 375(2089), 20160080, 2017.

Elgar, S., 1987, Relationships Involving Third Moment and Bispectra of a Harmonic Process, IEEE Transactions on Acoustics and Signal Processing, Vol. ASSP-35, No. 12, pp 1725-1726.

Hutchins and I Marusic. Evidence of very long meandering features in the logarithmic region of turbulent boundary layers. *J. Fluid Mech.*, 579:1–28, 2007a.

N. Hutchins and I. Marusic. Large-scale influences in near-wall turbulence. *Philos. Trans. R. Soc. A*, 365(1852):647–664, 2007b.

Kim, Y. C. and Powers, E. J., "Digital Bispectral Analysis and Its Applications to Nonlinear Wave Interactions," in *IEEE Transactions on Plasma Science,* vol. 7, no. 2, pp. 120-131, June 1979, doi: 10.1109/TPS.1979.4317207.

Lozier, M., Thomas, F.O., and Gordeyev, S. 2020. Streamwise Evolution of Turbulent Boundary Layer Response to Active Control Actuator. AIAA SciTech Forum, AIAA Paper 2020-0097.

Lozier, M., Thomas, F. O. and Gordeyev, S.V.,“Experimental Studies of Boundary Layer Dynamics via Active Manipulation of Large-Scale Structures,“ Procedings of the 12th Turbulent Shear Flow Phenomena (TSFP12), Osaka, Japan, 2022.

Mathis, R., Hutchins, N., and Marusic, I., 2009, Large-scale amplitude modulation of the small-scale structures in turbulent boundary layers, J. Fluid Mech., Vol. 681, p. 311.

Mathis, R., Marusic, I., Hutchins, N. and Sreenivasan, K. R., 2011, The relationship between the velocity skewness and the amplitude modulation of the small scale by the large scale in turbulent boundary layers, Physics of Fluids, 23, 121702.

Midya, S.,“On the spectral decomposition of skewness of streamwise velocity in a zero pressure gradient turbulent boundary layer,“ PhD Thesis, University of Notre Dame, 2021.

Rosenblatt, M.; Ness, J. W. Van. Estimation of the Bispectrum. Ann. Math. Statist. 36 (1965), no. 4, 1120--1136. doi:10.1214/aoms/1177699987.